Original Research Article

Numerical simulation of second-order stokes wave generation and propagation in a two-dimensional CFD wave flume

Liuhe Duan*, Baihuan Sun, Jie He
Power China Huadong Engineering Corporation Limited, Hangzhou, Zhejiang, 311122, China

Abstract: A two-dimensional computational wave flume was developed in ANSYS Fluent to examine the generation, propagation, and attenuation of regular waves imposed through a second-order Stokes inlet condition. The air-water interface was captured with the volume-of-fluid (VOF) method, and a downstream momentum-damping zone was used to reduce outlet reflection. The 120 m long, 9 m high flume had a still-water depth of 5 m and was discretized with 17,280 structured quadrilateral cells refined near the mean free surface. For a nominal wave height of 0.50 m and period of 2.50 s, the wave-gauge records exhibited a stable dominant period of approximately 2.5-2.6 s. The developed wave height was approximately 0.42-0.48 m at x = 5-15 m but decreased to 0.14-0.16 m at x = 95 m, corresponding to a reduction of about 60-70%. These results demonstrate stable temporal periodicity near the inlet but also substantial downstream attenuation. Consequently, grid/time-step convergence, analytical or experimental validation, and a quantitative reflection analysis are required before the model is used for wave-load prediction.
Keywords: numerical wave flume; second-order stokes wave; volume of fluid; wave generation; wave damping

1. Introduction

Numerical wave flumes are widely used to reproduce wave kinematics and hydrodynamic loading in coastal and offshore engineering. Compared with a closed laboratory testing, a computational flume provides direct access to the velocity, pressure, and phase fields and allows boundary conditions to be varied efficiently. A reliable numerical flume must nevertheless satisfy several requirements simultaneously: it must generate the prescribed incident wave, capture a sharply moving air-water interface, transmit the wave with limited numerical diffusion, and absorb outgoing wave energy without producing significant reflection [4-9].

For finite-amplitude regular waves, Stokes wave theory captures the nonlinear crest-trough asymmetry omitted by linear theory [1]. Within a two-phase Reynolds-averaged Navier-Stokes (RANS) framework, the volume-of-fluid (VOF) method represents the air-water interface by transporting a phase fraction [2]. This fixed-grid approach permits large interface motion, but its accuracy depends on spatial and temporal resolution, interface-compression treatment, turbulence closure, and consistency between the velocity and phase-fraction inlet conditions [4-6].

Recent studies have assessed relaxation zones, active-absorption boundaries, velocity-inlet formulations, and momentum-sink layers for numerical wave generation and absorption [5-9]. The common objective is to establish a stable periodic field while preventing reflected waves from contaminating the incident-wave region. The present study describes a two-dimensional regular-wave model in ANSYS Fluent and evaluates it using instantaneous phase distributions, longitudinal free-surface profiles, and time histories at ten monitoring locations. Particular attention is given to wave-train establishment, preservation of the dominant period, and spatial attenuation of wave amplitude.

2. Numerical method

2.1. Numerical formulation

The incompressible, two-phase Reynolds-averaged Navier-Stokes equations are solved. The VOF method transports the water volume fraction, and the free surface is represented by the water-volume-

fraction contour of 0.5. Mixture density and dynamic viscosity are computed by volume-fraction weighting. The SST k-ω model is used for turbulence closure.

The specified water density and dynamic viscosity are 998.2 kg m^{-3} and 1.003 × 10^{-3} Pa s, respectively, and gravitational acceleration is 9.81 m s^{-2}. The downstream wave-damping treatment enters the momentum equations as a sink term.

2.2. Wave generation and absorption

A regular wave based on second-order Stokes theory is imposed at the upstream velocity inlet with a nominal wave height of 0.50 m and period of 2.50 s. The inlet velocity components and water volume fraction are prescribed consistently with the selected wave theory, and the boundary forcing is ramped smoothly during start-up to reduce initial transients [1,8].

A pressure-outlet boundary is imposed at the downstream end. Immediately upstream, a damping zone applies a momentum sink to remove outgoing wave energy and reduce reflection. The zone length and coefficient distribution were selected for the target wave condition because absorption quality depends on both the damping formulation and its spatial configuration [6,7,9].

2.3. Computational domain and boundary conditions

The computational domain is a 120 m long and 9 m high rectangle. The still-water depth is 5 m, leaving a 4 m air region above the initial free surface. The upstream boundary is the wave-generation inlet, the downstream boundary is a pressure outlet, the upper boundary is maintained at atmospheric pressure, and the bottom is treated as a stationary no-slip wall. Initially, water occupies the region below y = 5 m and air occupies the region above it. **Figure 1** summarizes the geometry and boundary conditions.

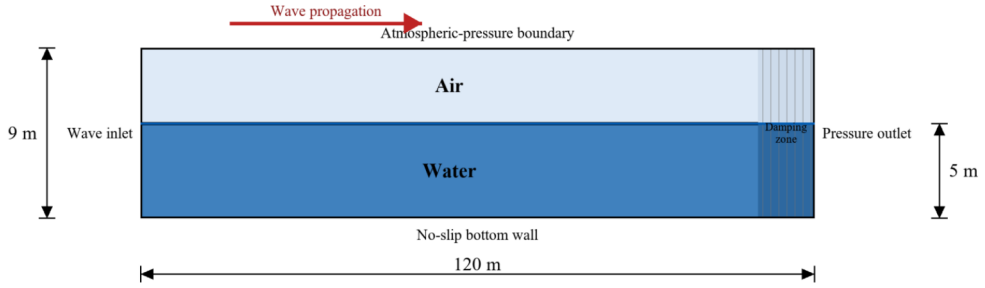
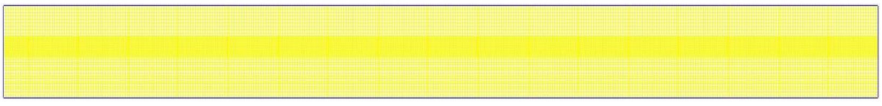


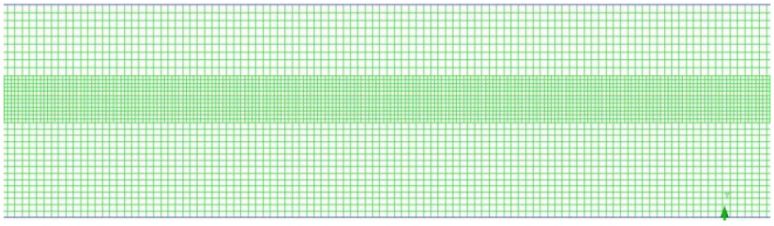
Figure 1. Geometry and boundary conditions of the two-dimensional numerical wave flume.

2.4. Mesh and solution settings

The rectangular domain is discretized with a structured quadrilateral mesh containing 17,280 fluid cells and 18,037 nodes. The maximum and minimum cell dimensions are approximately 0.333 and 0.166 m, respectively. Local refinement is applied over a band extending about one nominal wave height above and below the mean free surface to reduce interface smearing. The overall and locally refined meshes are shown in **Figure 2**.



(a)



(b)

Figure 2. Structured computational mesh: (a) overall domain and (b) local refinement near the mean free surface.

Pressure-velocity coupling uses the PISO algorithm [3]. PRESTO pressure interpolation, second-order spatial discretization for the momentum and turbulence-transport equations, and a compressive phase-fraction scheme are employed. The physical time step is 0.01 s, corresponding to approximately 250 time steps per nominal wave period. **Table 1** summarizes the principal parameters.

Table 1. Main computational and wave parameters.

Parameter	Value
Flume length	120 m
Total domain height	9 m
Still-water depth	5 m
Nominal wave height	0.50 m
Nominal wave period	2.50 s
Fluid cells	17,280
Time step	0.01 s
Turbulence model	SST k-ω
Simulation duration	100 s

3. Results and discussion

3.1. Development of the wave field

Figure 3 presents instantaneous phase distributions from t = 5 to 40 s. At t = 5 s, the disturbance remains concentrated near the upstream boundary and most of the downstream surface is nearly horizontal. At t = 10 and 15 s, the disturbed region extends downstream and additional crests and troughs appear behind the leading front. Between t = 20 and 30 s, the coherent wave train occupies an increasing part of the flume. By t = 35-40 s, regular oscillations are visible over almost the entire displayed domain.

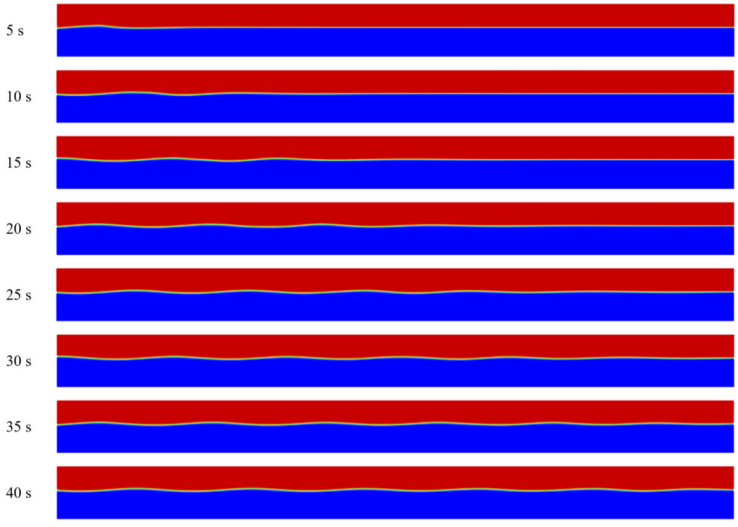


Figure 3. Instantaneous air-water phase distributions from t = 5 to 40 s; the interface is indicated by the yellow line.

The interface remains smooth throughout the start-up process, and the qualitative images show no visible overturning or breaking. Minor irregularities near the leading part of the wave packet diminish as the forcing becomes established.

3.2. Longitudinal free-surface profiles

The longitudinal profiles in **Figure 4** illustrate the spatial development of the wave field. The mean surface elevation remains close to the still-water level of 5 m. Within the developed part of the wave train, crest elevations are generally 5.20-5.28 m and trough elevations are approximately 4.72-4.80 m. These bounds imply local wave heights of about 0.40-0.56 m, compared with the nominal value of 0.50 m.

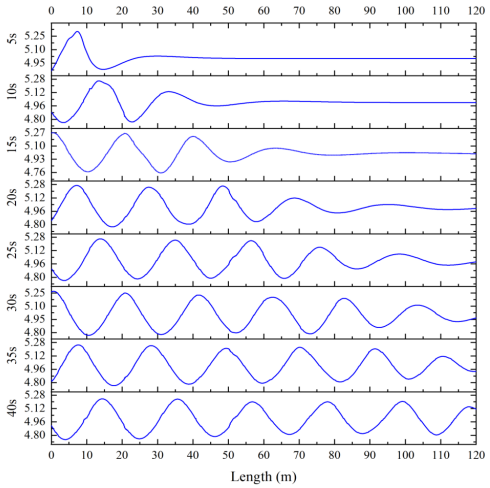


Figure 4. Longitudinal free-surface elevation profiles at selected times from 5 to 40 s.

The number of visible crests increases as the wave train propagates downstream. At intermediate times, weaker downstream oscillations may reflect both finite envelope development and accumulated dissipation. At t = 40 s, a coherent periodic profile occupies the plotted length, although the amplitude varies spatially. The mild crest-trough asymmetry is qualitatively consistent with a finite-amplitude Stokes wave [1].

3.3. Wave-gauge time histories and attenuation

Figure 5 shows free-surface time histories at monitoring points from x = 5 to 95 m in 10 m intervals. The onset of the developed oscillation is progressively delayed downstream. A stable periodic response is established within the first few seconds at x = 5 m, whereas the response at x = 95 m reaches its developed amplitude at approximately 45-50 s. Over the approximately 90 m gauge separation, this lag corresponds to an envelope-establishment velocity of about 2.0 m s^{-1}, close to the linear group velocity of 1.98 m s^{-1} for T = 2.50 s and h = 5 m. It should not be interpreted as the phase velocity of an individual crest.

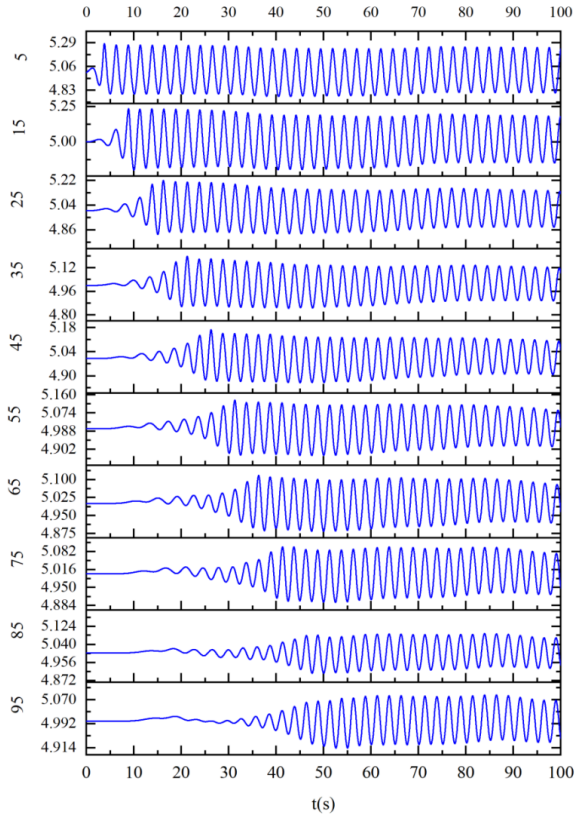


Figure 5. Time histories of the free-surface elevation at monitoring locations from x = 5 to 95 m.

After the initial transition, the gauges show an apparent dominant period of approximately 2.5-2.6 s, with no systematic frequency shift visible in the plotted records. The developed signals also appear regular, without sustained amplitude growth or long-period beating. These observations indicate temporal periodicity, but visual inspection alone cannot replace spectral and phase-error analyses or a quantitative reflection-coefficient estimate.

Once the oscillations are established, the wave amplitude generally decreases with distance. At x = 5-15 m, the amplitude is approximately 0.21–0.24 m, corresponding to a wave height of about 0.42–0.48 m. At x = 95 m, the amplitude decreases to approximately 0.07–0.08 m, corresponding to a wave height of about 0.14–0.16 m. Thus, the wave height at the downstream gauge is approximately 60–70% lower than that near the inlet. The observed attenuation may include both physical and numerical contributions, such as fluid viscosity, turbulence-model dissipation, interface smearing, and numerical diffusion [4]. Because only one mesh and one time-step size were considered, these contributions cannot be distinguished in the present results. The numerical flume produces a stable periodic signal and a near-target wave height close to the inlet. However, the 60-70% reduction in wave height over the monitored distance indicates that the present configuration does not provide high-fidelity, low-loss propagation. The qualitative absence of strong beating is encouraging but does not, by itself, establish effective reflection control.

The available results correspond to one mesh and one time step and include neither an analytical error assessment nor experimental validation. Consequently, they demonstrate the behavior of one numerical configuration rather than validate the model. Future work should compare multiple mesh and time-step levels, quantify phase and amplitude errors against analytical Stokes theory, and decompose incident and reflected components using a multi-gauge method. These checks are required before the flume is used for quantitative wave-load prediction.

4. Conclusions

A two-dimensional numerical wave flume based on the volume-of-fluid (VOF) method was developed to simulate regular wave generation and propagation. A second-order Stokes wave condition was applied at the inlet. The numerical results showed stable and periodic free-surface oscillations near the inlet, with no visible wave overturning or numerical instability during the simulation. The free-surface records obtained at all monitoring locations exhibited a dominant period of approximately 2.5–2.6 s, which was close to the prescribed wave period of 2.5 s. Near the inlet, the calculated wave height ranged from approximately 0.42 to 0.48 m, showing reasonable agreement with the prescribed value of 0.50 m. Meanwhile, the mean water level remained close to the initial still-water depth of 5 m. However, the wave amplitude decreased noticeably as the wave propagated downstream. At \(x=95\) m, the wave height decreased to approximately 0.14–0.16 m, corresponding to a reduction of about 60%–70% relative to the upstream monitoring locations. Overall, the results demonstrate the basic wave-generation and propagation characteristics of the present numerical configuration. Further investigation is still needed to assess its accuracy and general applicability.

About the author

*Corresponding author: Liuhe Duan(1991.10-), female, Han ethnicity, from Henan Province; Professional Title: Engineer; Educational Background: undergraduate course; Research Interests: Engineering Management; duan_lh@hdec.com.

References

[1] Fenton, J. D. (1985). A fifth-order Stokes theory for steady waves. Journal of Waterway, Port, Coastal, and Ocean Engineering, 111(2), 216-234. doi:10.1061/(ASCE)0733-950X(1985)111:2(216).

[2] Hirt, C. W., & Nichols, B. D. (1981). Volume of fluid (VOF) method for the dynamics of free boundaries. Journal of Computational Physics, 39(1), 201-225. doi:10.1016/0021-9991(81)90145-5.

[3] Issa, R. I. (1986). Solution of the implicitly discretised fluid flow equations by operator-splitting. Journal of Computational Physics, 62(1), 40-65. doi:10.1016/0021-9991(86)90099-9.

[4] Devolder, B., Rauwoens, P., & Troch, P. (2017). Application of a buoyancy-modified k-ω SST turbulence model to simulate wave run-up around a monopile subjected to regular waves using OpenFOAM. Coastal Engineering, 125, 81-94. doi:10.1016/j.coastaleng.2017.04.004.

[5] Windt, C., Davidson, J., & Ringwood, J. V. (2018). High-fidelity numerical modelling of ocean wave energy systems: A review of computational fluid dynamics-based numerical wave tanks. Renewable and Sustainable Energy Reviews, 93, 610-630. doi:10.1016/j.rser.2018.05.020.

[6] Choi, Y. M., Kim, Y. J., Bouscasse, B., Seng, S., Gentaz, L., & Ferrant, P. (2020). Performance of different techniques of generation and absorption of free-surface waves in computational fluid dynamics. Ocean Engineering, 214, 107575. doi:10.1016/j.oceaneng.2020.107575.

[7] Higuera, P. (2020). Enhancing active wave absorption in RANS models. Applied Ocean Research, 94, 102000. doi:10.1016/j.apor.2019.102000.

[8] Lv, C., Zhao, X., Li, M., & Xie, Y. (2022). An improved wavemaker velocity boundary condition for generating realistic waves in the numerical wave tank. Ocean Engineering, 261, 112188. doi:10.1016/j.oceaneng.2022.112188.

[9] Herdayanditya, I., Lataire, E., & Rauwoens, P. (2025). Spatial variations in numerical wave tanks with active wave generating-absorbing system. Ocean Engineering, 315, 119744. doi:10.1016/j.oceaneng.2024.119744.